



A constitutive model considering creep damage of wood

M. Trcala^{1,2} · P. Suchomelová¹ · M. Bošanský¹ · I. Němec³

Received: 28 October 2023 / Accepted: 19 February 2024 / Published online: 29 February 2024
© The Author(s) 2024

Abstract

The serviceability of wooden structures involves multiphysical phenomena, notably the interactions among creep, plasticity, and damage. The influence of creep on the initialization of the damage and on its growth and spread can be adjusted by an additional alpha parameter in order to take into account the coupled effect between creep and damage more properly. We integrate an orthotropic viscoelastic model, based on the generalized Kelvin chain, with an orthotropic damage model, capturing both the immediate nonlinear elastic–plastic–damage response and the time-dependent viscous response of timber. The combination of these material models is important to obtain a realistic description of wood behavior, because the timber shows an immediate nonlinear elastic–plastic–damage response, but also the time-dependent viscous response. In this paper, we algorithmize, implement, and validate the concept of ‘creep damage’, a phenomenon observed in wooden structures. Benchmark tests reveal two distinct patterns of damage in beech wood, immediate postload damage that evolves over time and damage that occurs and spreads during the loading period.

Keywords Wood · Time-dependent analysis · Viscoelasticity · Creep · Damage · Finite-element method · Numerical simulation

1 Introduction

The time-dependent behavior of wood has been widely observed, and the following measures of time-dependent response are commonly used in experimental investigations: creep, time-dependent deformation under constant load, relaxation, the stress decay under constant deformation, stiffness variation in dynamic mechanical analysis (Ferry 1980), and rate of loading (or straining) effects (Cannell and Morgan 1987). In current wood design standards, creep is considered using a serviceability criterion: the creep deflection is defined as a multiple of the dead-load deflection. However, creep can have a significant effect on the integrity of a structure. For example, long-term creep can magnify the short-term deflections

✉ P. Suchomelová
suchomelova.pav@gmail.com

¹ Faculty of Forestry and Wood Technology, Mendel University in Brno, Zemědělská 3, Brno, 613 00, Czechia

² Faculty of Civil Engineering, Brno University of Technology, Veveří 331/95, Brno, 602 00, Czechia

³ FEM Consulting, S.R.O., Veveří 331/95, Brno, 602 00, Czechia

in columns, compression panels, shallow arches, and shells through the geometric coupling of axial (membrane) and bending actions (the P-A effect). This can lead to the reduction of stiffness and buckling failures (Jones and Xirouchakis 1980; Holzer et al. 1989).

In common practice, it is usually assumed that wood exhibits a linear viscoelastic response for low load levels and that the instantaneous mechanical response of wood is elastic. For high loading levels, the deviation from the linearity of the creep behavior of wood is expected. Under high sustained loads, the cracks grow and interact with viscoelasticity. Some experimental and analytical results concerning nonlinear creep can be found in the literature for concrete (see among others Bazant and L'Hermite 1988; Bazant and Gettu 1992; Mazzotti and Savoia 2003; Omar et al. 2009; Dufour et al. 2006; Omar et al. 2004; Saliba et al. 2013); for wood, there are already fewer (Schniewind 1968; Hunt 1989; Massaro and Malo 2019).

During the service-life of wooden structures, wood is loaded and delayed strains appear due to the creep phenomenon. Some theories suggest that microcracks nucleate and grow when wood is submitted to a high sustained loading, thereby contributing to the weakening of wood. Thus, it is important to understand the interaction between viscoelastic deformation and damage to design reliable civil-engineering structures. Several creep-damage theoretical models have been proposed in the literature for concrete and most of these models are based on empirical relations applied at the macroscopic scale. Coupling between creep and damage is mostly realized by adding some parameters to consider the microstructure effects (see among others Bazant and L'Hermite 1988; Bazant and Gettu 1992; Mazzotti and Savoia 2003; Omar et al. 2009; Dufour et al. 2006; Omar et al. 2004; Saliba et al. 2013). In this paper, an orthotropic viscoelastic model is combined with an orthotropic damage model because the purpose of this paper is to demonstrate the time-dependent modeling of creep and damage of wood and the application of the finite-element method to predict the long-term creep-damage behavior of wooden structures by the finite-element method.

2 Theory

The objective of this study is to propose a model that allows us to couple the damage and the memory-dependent (viscous) behavior. The goal is to accurately predict the long-term behavior of the wooden structure. In this study, three models are provided: the pure viscoelastic model, the pure damage model, and the coupled viscoelastic–damage model.

2.1 Viscoelastic orthotropic model

The viscoelastic model is based on a generalized orthotropic Kelvin chain according to Bažant et al. (2018). Instead of the integral-type, the rate-type implementation with an exponential algorithm is utilized in this study, which can overcome two disadvantages from the integral-type mentioned above (Yu et al. 2012; Bažant et al. 2012; Toratti 1992; Liu 1994). The viscoelastic stress–strain relation can be approximated by a rheological model (e.g., Kelvin-chain model, Maxwell-chain model) in the rate-type algorithm (Bazant and Jirásek 2002; Hanhijärvi and Mackenzie-Helnwein 2003; Fortino et al. 2009; Massaro and Malo 2019). The Kelvin-chain model (Fig. 1) is implemented in this study which consists of a series of Kelvin chain units with coupled spring and dashpot. In rate-type implementation, by transferring the incremental stress–strain relation to a quasielastic incremental stress–strain relation, the creep calculation can be simplified to a series of elasticity problems with initial strains (Bažant et al. 2018; Bazant and Jirásek 2002; Hanhijärvi and Mackenzie-Helnwein

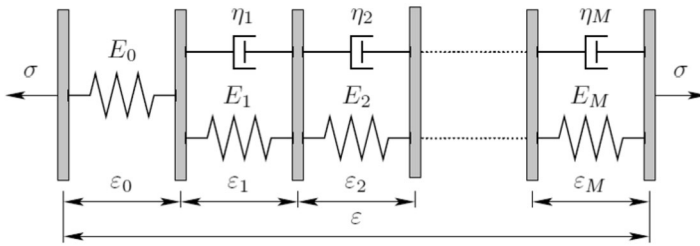


Fig. 1 Generalized Kelvin chain

2003; Fortino et al. 2009; Massaro and Malo 2019). Because of this simplification, the storage of previous data is no longer necessary, and the computational cost can be greatly reduced, which is important in large-scale structure analysis.

The presented model is based on plane stress conditions, but the extension to 3D is possible in the future. Assuming plane stress, the 2D stress tensor components are written in the following vector:

$$\boldsymbol{\sigma}^{(n)} \equiv \boldsymbol{\sigma}(t_n) = \begin{pmatrix} \sigma_x(t_n) \\ \sigma_y(t_n) \\ \tau_{xy}(t_n) \end{pmatrix} \equiv \begin{pmatrix} \sigma_L(t_n) \\ \sigma_R(t_n) \\ \tau_{LR}(t_n) \end{pmatrix}. \tag{1}$$

The stress at time t_n marked as $\boldsymbol{\sigma}^{(n)}$ is calculated using the known stress at time t_{n-1} marked as $\boldsymbol{\sigma}^{(n-1)}$ and the stress increment $\Delta\boldsymbol{\sigma}$:

$$\boldsymbol{\sigma}^{(n)} = \boldsymbol{\sigma}^{(n-1)} + \Delta\boldsymbol{\sigma}. \tag{2}$$

The stress increment is calculated according to Bazant and Jirásek (2002):

$$\Delta\boldsymbol{\sigma} = \mathbf{C}^{ve} : (\Delta\boldsymbol{\varepsilon} - \Delta\boldsymbol{\varepsilon}^v), \tag{3}$$

where the viscoelastic stiffness matrix \mathbf{C}^{ve} is the inverse of the viscoelastic compliance matrix \mathbf{D}^{ve} :

$$\mathbf{C}^{ve} = (\mathbf{D}^{ve})^{-1} = \begin{bmatrix} \frac{E_L^{ve}}{1-\nu_{LR}\nu_{RL}} & \frac{\nu_{LR}E_R^{ve}}{1-\nu_{LR}\nu_{RL}} & 0 \\ \frac{\nu_{RL}E_L^{ve}}{1-\nu_{LR}\nu_{RL}} & \frac{E_R^{ve}}{1-\nu_{LR}\nu_{RL}} & 0 \\ 0 & 0 & G_{LR}^{ve} \end{bmatrix}, \tag{4}$$

where

$$\mathbf{D}^{ve} = \begin{bmatrix} \frac{1}{E_L^{ve}} & \frac{-\nu_{LR}}{E_R^{ve}} & 0 \\ \frac{-\nu_{RL}}{E_L^{ve}} & \frac{1}{E_R^{ve}} & 0 \\ 0 & 0 & \frac{1}{G_{LR}^{ve}} \end{bmatrix}. \tag{5}$$

The viscoelastic compliance matrix \mathbf{D}^{ve} is assembled from the effective viscoelastic moduli, which were calculated from the following 1D relations (Bazant and Jirásek 2002):

$$\begin{aligned}
 E_L^{ve} &= \left(\frac{1}{D_{L0}} + \sum_{j=1}^M \frac{1 - \lambda_{Lj}}{D_{Lj}} \right)^{-1}, & E_R^{ve} &= \left(\frac{1}{D_{R0}} + \sum_{j=1}^M \frac{1 - \lambda_{Rj}}{D_{Rj}} \right)^{-1}, \\
 G_{LR}^{ve} &= \left(\frac{1}{D_{LR0}} + \sum_{j=1}^M \frac{1 - \lambda_{LRj}}{D_{LRj}} \right)^{-1} \\
 \tau_{Lj} &= \frac{\eta_{Lj}}{E_{Lj}}, & \beta_{Lj} &= \exp\left(\frac{-\Delta t}{\tau_{Lj}}\right), & \lambda_{Lj} &= \frac{\tau_{Lj}}{\Delta t} (1 - \beta_{Lj}) \\
 \tau_{Rj} &= \frac{\eta_{Rj}}{E_{Rj}}, & \beta_{Rj} &= \exp\left(\frac{-\Delta t}{\tau_{Rj}}\right), & \lambda_{Rj} &= \frac{\tau_{Rj}}{\Delta t} (1 - \beta_{Rj}), \\
 \tau_{LRj} &= \frac{\eta_{LRj}}{G_{LRj}}, & \beta_{LRj} &= \exp\left(\frac{-\Delta t}{\tau_{LRj}}\right), & \lambda_{LRj} &= \frac{\tau_{LRj}}{\Delta t} (1 - \beta_{LRj})
 \end{aligned} \tag{6}$$

where τ [s] is the retardation time and η [Pa s] is viscosity.

The increment of the viscous strain vector is calculated in 2D as follows:

$$\Delta \boldsymbol{\varepsilon}^v = \Delta t \sum_{j=1}^M \begin{pmatrix} \lambda_{Lj} \frac{d\varepsilon_{Lj}^{(n-1)}}{dt} \\ \lambda_{Rj} \frac{d\varepsilon_{Rj}^{(n-1)}}{dt} \\ \lambda_{LRj} \frac{d\gamma_{LRj}^{(n-1)}}{dt} \end{pmatrix}, \tag{8}$$

where the state variables calculated at the previous time t_{i-1} are used: $\frac{d\varepsilon_{Lj}^{(n-1)}}{dt}$, $\frac{d\varepsilon_{Rj}^{(n-1)}}{dt}$, $\frac{d\gamma_{LRj}^{(n-1)}}{dt}$.

These state variables are needed to update and to calculate the next time step:

$$\begin{aligned}
 \frac{d\varepsilon_{Lj}^{(n)}}{dt} &= \beta_{Lj} \frac{d\varepsilon_{Lj}^{(n-1)}}{dt} + \frac{1 - \beta_{Lj}}{\Delta t D_{Lj}} \Delta \sigma_L \\
 \frac{d\varepsilon_{Rj}^{(n)}}{dt} &= \beta_{Rj} \frac{d\varepsilon_{Rj}^{(n-1)}}{dt} + \frac{1 - \beta_{Rj}}{\Delta t D_{Rj}} \Delta \sigma_R \\
 \frac{d\gamma_{LRj}^{(n)}}{dt} &= \beta_{LRj} \frac{d\gamma_{LRj}^{(n-1)}}{dt} + \frac{1 - \beta_{LRj}}{\Delta t D_{LRj}} \Delta \tau_{LR}
 \end{aligned} \tag{9}$$

The retardation time of the j th unit of the Kelvin chain in a given material direction is the ratio of the corresponding viscosity and modulus of elasticity of the j th unit in the given material direction. These viscosities and elasticity moduli must be determined (fitted) from known measured creep curves (creep-strain dependency on time) in the given material directions of the wood. An algorithm based on the Particle-Swarm Optimization method is used in this study (Kennedy and Eberhart 1995; Shi and Eberhart 1998).

2.2 The orthotropic damage model

The damage model for orthotropic wood material has been taken from the literature (Sandhaas et al. 2020; Maimí et al. 2007, 2006; Matzenmiller et al. 1995). In these sources, a brief description of this damage model with respect to 2D plane stress is given. It is assumed that the linear elastic stiffness matrix C_{ijkl}^e is constant over time and the damage stiffness matrix only is reduced to $C_{ijkl}^{dam}(t_n)$.

The linear elastic stress predictor is the following:

$$\sigma_{ij}^e(t_n) = C_{ijkl} \varepsilon_{kl}(t_n), \tag{10}$$

the resulting stress is calculated as follows:

$$\sigma_{ij}(t_n) = C_{ijkl}^{dam}(t_n) \varepsilon_{kl}(t_n) \tag{11}$$

and the damage criteria are defined according to Sandhaas et al. (2020), Maimí et al. (2007, 2006), Matzenmiller et al. (1995):

$$\mathbf{F} - \boldsymbol{\kappa} = \mathbf{0}. \tag{12}$$

The Kuhn–Tucker and consistency conditions must hold (Sandhaas et al. 2020):

$$\mathbf{F} - \boldsymbol{\kappa} \leq \mathbf{0}, \quad \frac{d\boldsymbol{\kappa}}{dt} \geq \mathbf{0}, \quad \frac{d\boldsymbol{\kappa}}{dt} (\mathbf{F} - \boldsymbol{\kappa}) = 0. \tag{13}$$

The damage-evolution functions, state variables $\boldsymbol{\kappa}$ are introduced, which keep track of the loading history (Sandhaas et al. 2020; Maimí et al. 2006).

If $F_{ij}(t_n) > 1$, then

$$\kappa_{ij}(t_n) = \max \{ F_{ij}(t_n), \kappa_{ij}(t_{n-1}) \}$$

else

$$\kappa_{ij}(t_n) = 1,$$

or, simplest

$$\kappa_{ij}(t_n) = \max \{ 1, F_{ij}(t_n), \kappa_{ij}(t_{n-1}) \}. \tag{14}$$

The damage parameters are calculated from these state variables according to Sandhaas et al. (2020), Maimí et al. (2006):

$$d_{ij}(t_n) = d_{ij}(\kappa_{ij}(t_n)). \tag{15}$$

The constitutive stiffness damage matrix is then calculated as the inverse of the compliance damage matrix:

$$C_{ijkl}^{dam} = \begin{bmatrix} \frac{1}{(1-d_L)E_L} & \frac{-\nu_{LR}(d_L, d_R, d_{LR})}{(1-d_R)E_R} & 0 \\ \frac{-\nu_{RL}(d_L, d_R, d_{LR})}{(1-d_L)E_L} & \frac{1}{(1-d_R)E_R} & 0 \\ 0 & 0 & \frac{1}{(1-d_{LR})G_{LR}} \end{bmatrix}^{-1}. \tag{16}$$

This damage model is used for the description of both the brittle and ductile (plastic) behavior of wood using the specific state variables.

2.3 Viscoelastic–damage model

The viscoelastic–damage model is proposed, where the instantaneous behavior and memory-dependent (viscous) behavior are considered. Therefore, the total strain tensor can be decomposed into the instantaneous strain tensor and the memory-dependent strain tensor. The instantaneous strain tensor, including the elastic-strain tensor and plastic- or damage-strain tensor, will develop instantaneously after loading, while the memory-dependent strain tensor, including viscous measures like creep, will grow with time. The additive decomposition of the total strain tensor can be used while assuming small deformations:

$$\varepsilon_{kl}(t) = \varepsilon_{kl}^e(t) + \varepsilon_{kl}^p(t) + \varepsilon_{kl}^d(t) + \varepsilon_{kl}^c(t), \tag{17}$$

where $\varepsilon_{kl}^e(t)$ is the instantaneous elastic, $\varepsilon_{kl}^p(t)$ is the instantaneous plastic, $\varepsilon_{kl}^d(t)$ is the instantaneous damage, and $\varepsilon_{kl}^c(t)$ is the memory-dependent (viscous) component – for example, creep strain.

The components of the stress tensor are calculated under the assumption that the instantaneous elastic component of the strain tensor is not only elastic but also linear and Hooke’s law is applied. In the case of wood, the yield strength is equal to the linear limit – therefore, nonlinear elasticity does not occur, and elasticity can always be considered to be linear:

$$\sigma_{ij}(t) = C_{ijkl}^e \varepsilon_{kl}^e(t), \tag{18}$$

where C_{ijkl}^e is the constitutive stiffness matrix of the orthotropic material according to Hooke’s law. It is assumed that it does not change over time.

If the linear elastic component of the strain is expressed from the relation (17) and we substitute it into the relation (18), we obtain the following form for calculating the stress components:

$$\sigma_{ij}(t) = C_{ijkl}^e (\varepsilon_{kl}(t) - \varepsilon_{kl}^p(t) - \varepsilon_{kl}^d(t) - \varepsilon_{kl}^c(t)). \tag{19}$$

It is appropriate to point out that the damage component of the deformation is usually calculated from the so-called damage parameters, which modify the original elastic constitutive stiffness matrix, and damage deformation can then be calculated from these damage parameters, and if this damage model is also used considering the plastic behavior, the plastic component of the deformation can also be calculated from it, and the following applies:

$$\varepsilon_{kl}^p(t) + \varepsilon_{kl}^d(t) = \varepsilon_{kl}(t) - \varepsilon_{kl}^c(t) - [C_{ijkl}^e]^{-1} \sigma_{ij}(t), \tag{20}$$

where individual stress components are calculated using a damage matrix $C_{ijkl}^{dam}(t)$:

$$\sigma_{ij}(t) = C_{ijkl}^{dam}(t) (\varepsilon_{kl}(t) - \varepsilon_{kl}^c(t)). \tag{21}$$

The goal is to design, implement, and validate a numerical algorithm (numerical integration over time), that combines the two mentioned models:

- a) the viscoelastic model;
- b) the damage model.

At the given time t_n , i.e., at the end of the time step $\langle t_{n-1}, t_n \rangle$ of size $\Delta t = t_n - t_{n-1}$ in each iteration of the global Newton method, the procedure is as follows (in each iteration, only the increment of the total strain $\Delta \boldsymbol{\varepsilon}$ is a variable input from the solver, otherwise the other quantities are constant and their values are taken from the previous converged time t_{n-1}):

The creep model (generalized Kelvin chain) is applied, and the viscoelastic stress increment is calculated according to the relation:

$$\Delta\sigma^{ve} = \mathbf{C}^{ve} : (\Delta\boldsymbol{\varepsilon} - \Delta\boldsymbol{\varepsilon}^v) \tag{22}$$

and the resulting creep-strain increment is then calculated as follows:

$$\Delta\boldsymbol{\varepsilon}^c = \Delta\boldsymbol{\varepsilon} - \mathbf{D}^e : \Delta\sigma^{ve}, \tag{23}$$

where $\mathbf{D}^e = [\mathbf{C}^e]^{-1}$ is the linear elastic compliance matrix. Due to the use of the Kelvin chain, this calculation depends only on the state variables from the previous time t_{i-1} in the first iteration.

The damage model is used, and the resulting stresses and constitutive stiffness matrices are calculated, which already leads to the global finite-element system of equations. Within the framework of Newton’s method, another iteration can be performed to find the balance approximately gradually between the internal and external nodal forces of the entire structure under investigation.

The basic idea is that the total strain reduced by the viscous strain (creep strain) leads to the damage model, but that a certain creep component participates in the calculation of damage parameters according to this relation:

$$\boldsymbol{\varepsilon}^{vin}(t_n) = \boldsymbol{\varepsilon}^{in}(t_n) + \alpha\boldsymbol{\varepsilon}^c(t_n) \tag{24}$$

or in incremental form:

$$\Delta\boldsymbol{\varepsilon}^{vin} = \Delta\boldsymbol{\varepsilon}^{in} + \alpha\Delta\boldsymbol{\varepsilon}^c, \tag{25}$$

where $\boldsymbol{\varepsilon}^{in}(t_n) = \boldsymbol{\varepsilon}(t_n) - \boldsymbol{\varepsilon}^c(t_n) - \boldsymbol{\varepsilon}^M(t_n) - \boldsymbol{\varepsilon}^T(t_n) - \dots$ is the instantaneous strain tensor because it corresponds to the immediate (elastic–plastic–damage) response of the material.

In this damage model, the total strain is reduced by the creep strain (like by other time-dependent initial strains, e.g., from moisture $\boldsymbol{\varepsilon}^M$ or temperature changes) $\boldsymbol{\varepsilon}^T$ but into the damage model enters not only instantaneous strain but also the creep strain (viscous) component according to equation (23). Let us call $\boldsymbol{\varepsilon}^{vin}$ the viscous instantaneous component of total strain including not only instantaneous strain but also the creep-strain component. The proportion of creep strain $\boldsymbol{\varepsilon}^c$ to viscous instantaneous strain $\boldsymbol{\varepsilon}^{vin}$ is given by the alpha parameter α .

Let us denote the nonlinear part of the instantaneous strain as $\boldsymbol{\varepsilon}^d$ (damage or plasticity) and then the instantaneous strain is equal to the linear (elastic) strain plus the strain corresponding to the nonlinearity (damage):

$$\boldsymbol{\varepsilon}^{in} = \boldsymbol{\varepsilon}^e + \boldsymbol{\varepsilon}^d, \tag{26}$$

where $\boldsymbol{\varepsilon}^e = \mathbf{D}^e : \boldsymbol{\sigma}$ and $\boldsymbol{\varepsilon}^d$ is the strain mentioned above, e.g., from damage, which is still unknown, as well as the resulting stress $\boldsymbol{\sigma}$, but both will be calculated using the damage model.

A linear elastic stress prediction can then be performed using this introduced viscous instantaneous strain $\boldsymbol{\varepsilon}^{vin}(t_n)$:

$$\boldsymbol{\sigma}^{vin}(t_n) = \mathbf{C} : \boldsymbol{\varepsilon}^{vin}(t_n). \tag{27}$$

The damage parameters can be calculated using these modified (viscous instantaneous) stresses and creep strain, which means that the damage parameters are now functions of

the viscous instantaneous strain, which was created by modifying the instantaneous (time-independent) strain by a component of the viscous (time-dependent) strain:

$$\mathbf{D} = \mathbf{f}(\boldsymbol{\sigma}^{vin}) \quad (28)$$

and their calculation is carried out in a standard way, as described above (Sandhaas et al. 2020).

The resulting stress tensor is then obtained according to the common relation:

$$\begin{aligned} \boldsymbol{\sigma}(t_n) &= \mathbf{C}^{dam}(t_n) : \boldsymbol{\varepsilon}^{in}(t_n) \\ &= (\mathbf{I} - \mathbf{D}(\boldsymbol{\sigma}^{vin}(t_n))) : \mathbf{C}^e : \boldsymbol{\varepsilon}^{in}(t_n) \\ &= (\mathbf{I} - \mathbf{D}(\boldsymbol{\sigma}^{vin}(t_n))) : \mathbf{C}^e : (\boldsymbol{\varepsilon}(t_n) - \boldsymbol{\varepsilon}^c(t_n)). \end{aligned} \quad (29)$$

The following options were tested for the stiffness tensor, which is used to calculate the strain increment in the next iteration within the global Newton method:

$$\mathbf{C} = \mathbf{C}^{ve}, \quad \mathbf{C} = \mathbf{C}^{dam}, \quad \mathbf{C} = \mathbf{C}^e \quad (30)$$

and the best convergence was achieved with this first viscoelastic option $\mathbf{C} = \mathbf{C}^{ve}$.

The strain that belongs to the damage model can be calculated using the resulting stress according to following form:

$$\boldsymbol{\varepsilon}^d(t_n) = \boldsymbol{\varepsilon}(t_n) - \boldsymbol{\varepsilon}^c(t_n) - \boldsymbol{\varepsilon}^e(t_n) = \boldsymbol{\varepsilon}(t_n) - \boldsymbol{\varepsilon}^c(t_n) - \mathbf{D}^e : \boldsymbol{\sigma}(t_n). \quad (31)$$

This theory is inspired by the model for concrete (Mazzotti and Savoia 2003), where the creep strains are the components of the total strains, and they are weighted by an intensity factor α , which is included in the equivalent strain.

3 Methods

In this study, pure viscoelastic, pure damage, and coupled viscoelastic–damage models are implemented into Dlubal RFEM software. The model was algorithmized, programmed, implemented, and numerically validated into this finite-element method software. The implementation is based on the extension of its material library.

First, the material properties of beech wood are listed, which are divided into a) time-independent, b) time-dependent (viscous) and, as the second point, the list of the Dual benchmark tasks, which show the behavior of the given material model on different structures (various geometry, boundary conditions such as loads or supports).

3.1 Material properties of wood

The list of time-independent properties (elastic–plastic–damage properties) is given in Table 1 and Fig. 2.

The stiffness properties used refer to the plane LR . This approximation is suitable for most of the listed properties, except for the transversal modulus of elasticity. Indeed, several studies show that if we approximate an element, which is described by a cylindrical set of properties, with an equivalent set of Cartesian properties (x, y, z), then the modulus in the vertical direction (E_{90}) is lower than both E_R and E_T . It does not affect the working principle

Table 1 Time independent properties of wood (Ozyhar et al. 2013; Bengtsson et al. 2022)

LINEAR MATERIAL PROPERTIES

Tensile strength

$F_{t,0}$ (parallel to the grain)	41 MPa
$F_{t,90}$ (perpendicular to the grain)	4.3 MPa

Compressive strength

$F_{c,0}$ (parallel to the grain)	45 MPa
$F_{c,90}$ (perpendicular to the grain)	14.2 MPa

Shear strength

F_v	6.9 MPa
-------	---------

Modulus of elasticity

$E_{L,t0}$	10 459 MPa
$E_{R,t0}$	1480 MPa

Shear modulus

$G_{RL,t0}$	900 MPa
-------------	---------

Poisson ratios

$\nu_{RL,t0}$	0.24
---------------	------

NONLINEAR MATERIAL PROPERTIES

Fracture energy (tensile)

$G_{f,0}$ (parallel to the grain)	100 000 N/m
$G_{f,90}$ (perpendicular to the grain)	710 N/m
$G_{f,v}$ (shear)	1200 N/m

of the presented model, but in order to calibrate the model with experimental results, a more accurate value should be used in later works.

For the nondiagonal elements of the wood compliance matrix several studies (Ozyhar et al. 2013) have pointed out that significant discrepancies can occur in the values of these nondiagonal elements. In these studies, for simplicity reasons, these values, based on the orthotropic symmetry of compliance are assumed as equal. In the future work, we can discuss the mechanics behind the time-dependent behavior of Poisson’s ratios based on the orthotropic symmetry and its development with time for the LR and LT planes.

The time-dependent properties (viscoelastic properties) such as creep curves and Kelvin-chain parameters are given in Fig. 3 and below.

The creep curves (Fig. 3) are used to fit the parameters of the orthotropic Kelvin chain, and further, to represent the viscoelastic component of the wood material model.

From a practical point of view it is therefore necessary to use the creep functions as an input of the model instead of M unknown pairs of E_j and τ_j . The implemented algorithm for the identification of the Kelvin-chain parameters is designed to work with the creep function, which is inverse to the above-mentioned compliance function. The approximation of the creep function via the Dirichlet series was modified, for the algorithm, into the following form:

$$\varphi(t) = 1 + \sum_{j=1}^M E_j \left(1 - e^{-\frac{t}{\tau_j}}\right). \tag{32}$$

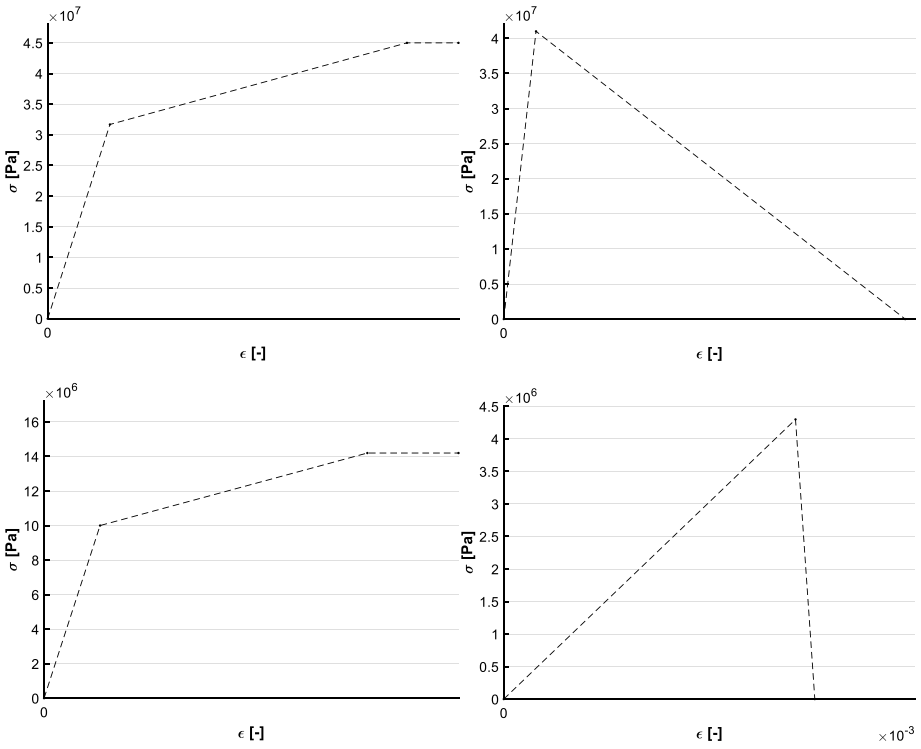


Fig. 2 Bilinear/trilinear material model with hardening a) compressive ductile (hardening) (upper left – longitudinal, lower left – transversal), b) tensional brittle (softening) behavior (upper right – longitudinal, lower right – transversal)

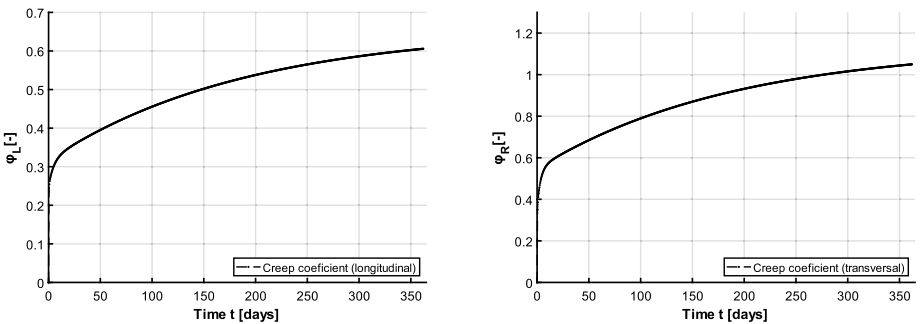


Fig. 3 The set of experimental creep tests were taken from Bažant and Wu (1973), Moll et al. (1991)

The problem of identification of unknown coefficients of series from experimental data was described by Bažant and Wu (1973) who proved the use of the least-squares method (LSM) for the determination of E_j , where the values of retardation times τ_j had been chosen empirically to ensure even coverage of the time axis on a logarithmic scale. Complete identification of all parameters is possible to determine as roots of polynomials, whose coefficients are determinants of the matrices that are obtained from the values of approximated

creep function and its derivatives (Moll et al. 1991). The identification can also be formulated as an optimization task. This approach is described in the work of Distéfano (1970) and Pister (1972). These authors solved the identification problem as nonlinear optimization. Concerning actual computing power, it is possible to use more demanding modern optimization algorithms based on imitation of natural processes. This idea is used within the designed algorithm where optimization is solved using the Particle-Swarm strategy (Kennedy and Eberhart 1995; Shi and Eberhart 1998).

The implemented identification algorithm is a combination of Bažant's proposed LSM with empirically determined values of τ_j and optimization where these values are refined to obtain an as accurate approximation of the user-defined creep curve as possible. The objective function is defined as an RMSE error as follows:

$$\text{RMSE} = \sqrt{\frac{\sum_{i=1}^n (y_i^* - y_i)^2}{n}}, \quad (33)$$

where y_i^* is the creep coefficient value obtained using the Dirichlet series and y_i is the creep-coefficient value defined by the user and n is a number of points. Optimization constraints were defined by the following inequalities:

$$0.9\tau_j \leq \tau_j^* \leq 1.1\tau_j, \quad (34)$$

where τ_j is the value of the empirically estimated retardation time and τ_j^* is the value of the retardation time obtained using the Particle-Swarm optimization algorithm.

The best results were achieved for approximation with 5 Kelvin–Voight models in series. The averaged RMSE errors have reached values of $0.001266289 \pm 1.27 \times 10^{-4}$ for L and $0.002733644 \pm 2.84 \times 10^{-4}$ for R . Realizations for 5 members are graphically indistinguishable from the input curves. In the case of 7 and 9 members the results were also numerically and graphically accurate enough but the average time consumption for the calculation of single identification is 1.7 times higher for 7 members and 2.6 higher for 9 members. These above-mentioned results were used to decide to use 5 members of the chain for structural analyses.

3.2 Benchmark tests methods

The benchmark tasks, which were used to test and analyze the new material model combining the viscoelastic and the damage models are the following:

A1, A2, B, and C are represented as a simple wall shell of $1 \times 1 \times 1$ m. Geometry D is a beam represented as a shell structure under 2D plane-stress assumptions. The dimensions of the beam are $0.36 \times 0.02 \times 0.02$ m, the supports distance is 0.3 m. The geometry E is also a beam shell structure, but with dimensions of $0.91 \times 0.07 \times 0.045$ m, the supports distance is 0.8 m, see Fig. 4.

The boundary conditions marked as u are displacement boundary conditions in the x , y , and z directions. On the other hand, the boundary conditions marked as φ are rotation boundary conditions around the orthotropic x , y , and z directions. Walls A1 and A2 have one fixed boundary and the opposite boundary loaded by 30 kN/m (A1) and 40 kN/m (A2). They represent the time-dependent response of wood to the compressive loading in longitudinal direction. The wall structure B shows the bending behavior of the shell structure with two opposite boundaries fixed and the perpendicular surface load. Task C also represents the same bending test as task B, but with four boundaries fixed. The task D shows the 2D plane

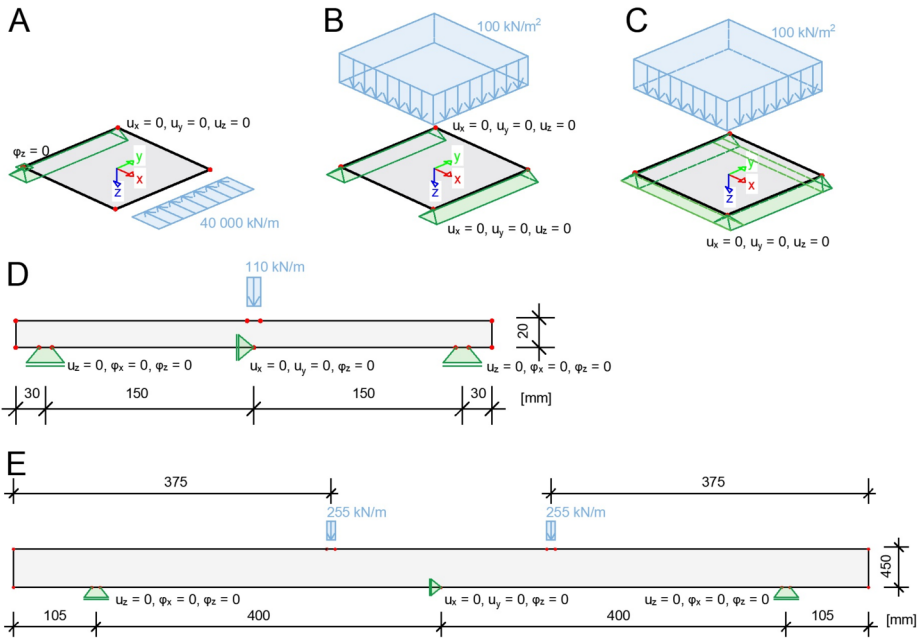


Fig. 4 Overview of the benchmark tasks (Color figure online)

stress model of the beam structure to show the example of three-point bending with short line boundary conditions representing the supports of the beam and short line load in the middle of the beam length. As for D, the task E is a beam structure, with the difference of being loaded in four-point bending. The supports and load are also applied on short lines.

4 Results

The aim is to represent the behavior of the new material model with the newly introduced alpha parameter on the resulting time response of selected benchmark tasks. For this reason, the influence of the alpha parameter on the time curves is shown on the first benchmark tasks (task A) by comparing the results with a material model without the alpha parameter and with a material model without damage, i.e., purely viscoelastic. The significant influence of the alpha parameter is demonstrated in the first tasks (Figs. 5, 6, 7, and 9), and therefore, the behavior of the material model under different loading levels is shown only with a nonzero alpha parameter in Figs. 8, 10, 11, 12, 13, and 14.

Figure 5 shows the time course of displacement in the longitudinal direction of the wood in two different loading levels. For both of these loading levels, the task is calculated using three cases of the material model: a) the linear viscoelastic model without the influence of the damage (generalized Kelvin chain), b) the viscoelastic model in combination with the damage model (Kelvin chain + damage model) without considering the alpha parameter, c) the viscoelastic model in combination with the damage model (Kelvin chain + damage model) with a nonzero alpha parameter set to 0.4.

It is observed that at a lower load level (30 MPa; just below the yield point of wood) the damage (plasticity) does not occur immediately after loading, but only after a certain time

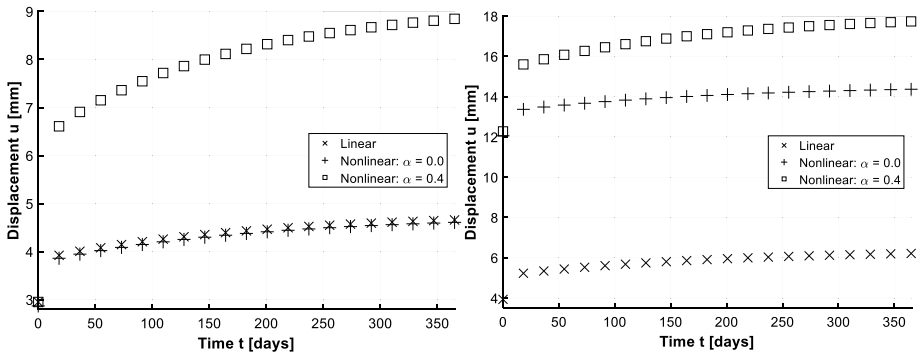


Fig. 5 Results of benchmark tasks A1 and A2: the displacement u in the longitudinal direction of the wood in two different loading levels (30 MPa – left, 40 MPa – right)

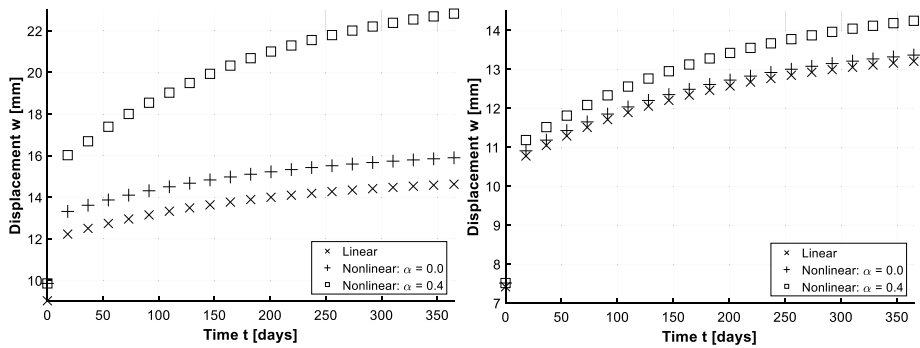


Fig. 6 Results of benchmark tasks B and C: the deflection (displacement w) of the shell structure loaded by 615 kN/m^2 in the transversal direction a) supported on both sides (left), b) supported on all four sides (right)

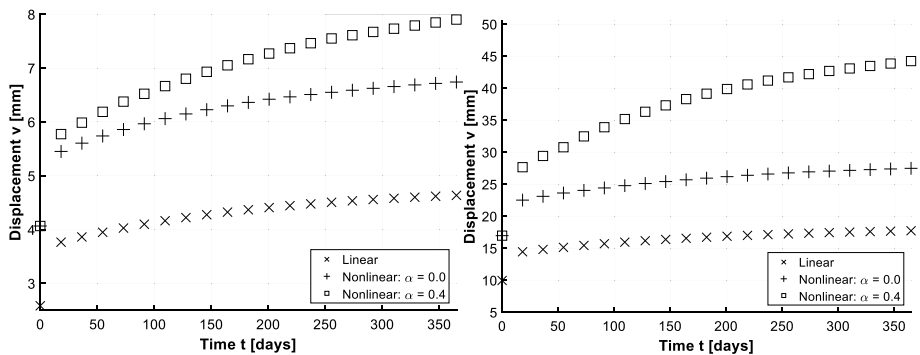


Fig. 7 Results of benchmark tasks D and E: the beam deflection (displacement v in the transversal y direction), a) three-point bending test, line loading of 100 kN/m (left), b) four-point bending test, two lines load of $2 \times 240 \text{ kN/m}$ (right)

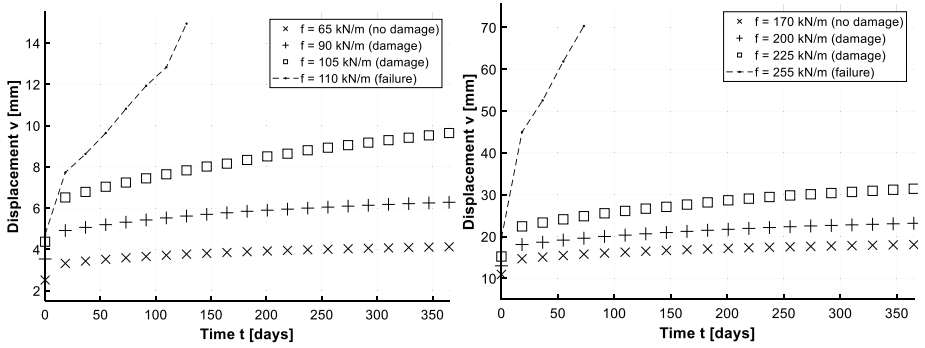


Fig. 8 Results of benchmark tasks D and E: deflection (displacement v in the transversal y direction) for different loading levels f with the alpha parameter a) three-point bending test (left), b) four-point bending test (right)

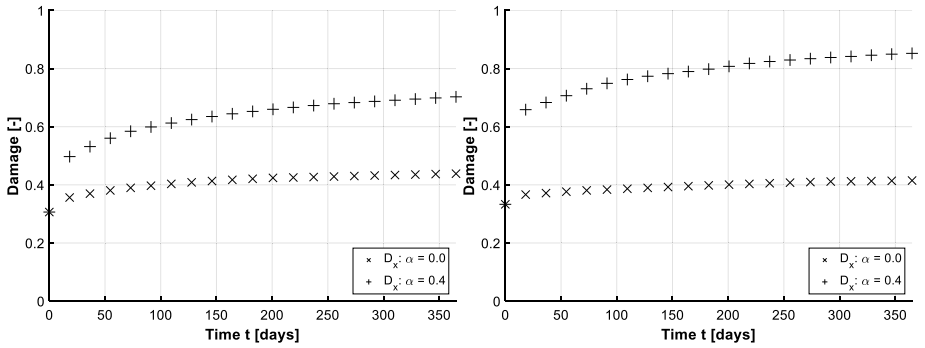


Fig. 9 Results of benchmark tasks D and E: beam deflection (displacement v in the transversal y direction) for a) three-point bending test, line load 100 kN/m (left), b) four-point bending test, two lines load 2×250 kN/m (right)

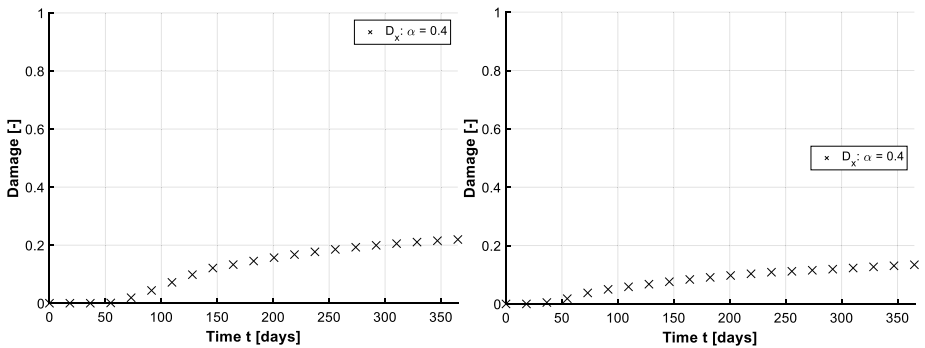


Fig. 10 Results of benchmark tasks D and E: beam deflection (displacement v in the transversal y direction), use of the alpha parameter for a) three-point bending test, line load of 70 kN/m (left), b) four-point bending test, two lines load of 2×180 kN/m (right)

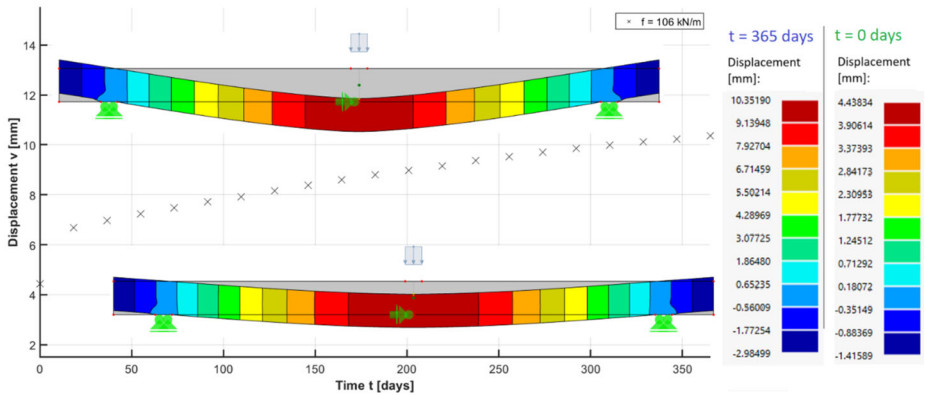


Fig. 11 Deflection of the beam during three-point bending test with line load 106 kN/m immediately after load application (0 days, below) and after 365 days of loading (above) (Color figure online)

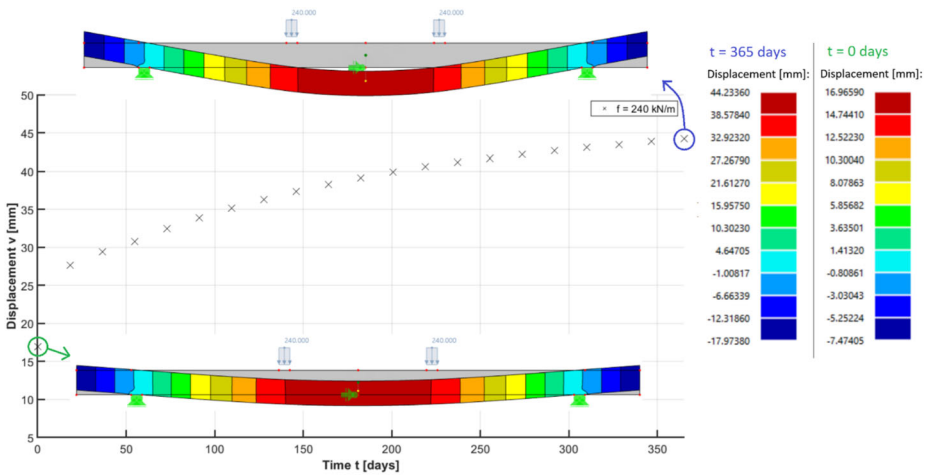


Fig. 12 Deflection of the beam during four-point bending test with two lines load 2×240 kN/m immediately after load application (0 days, below) and after 365 days of loading (above) (Color figure online)

has passed due to creep, and only with nonzero parameter $\alpha = 0.4$, because this is a case of uniaxial stress, where a constant external load is prescribed. Without the influence of the α parameter, the yield strength cannot be exceeded (Fig. 5, left). On the other hand, it can be seen that at a higher load, the yield strength will be exceeded right at the beginning after the load application, and this damage increases over time both in the case of $\alpha = 0.4$ and also in the case of $\alpha = 0$, because the damage response (plasticity) occurred at the very beginning and increases with creep even without the influence of the α parameter (Fig. 5, right). The importance and influence of the α parameter on the occurrence and development of damage (plasticity) over time as a result of the phenomenon of creep damage is shown here.

Figure 6 shows the application of the material model on the plates supported on both sides (left, task B) and supported on all four sides (right, task C). This plate is loaded with a continuous surface load of 615 kN/m^2 . The diagram shows the time courses of the de-

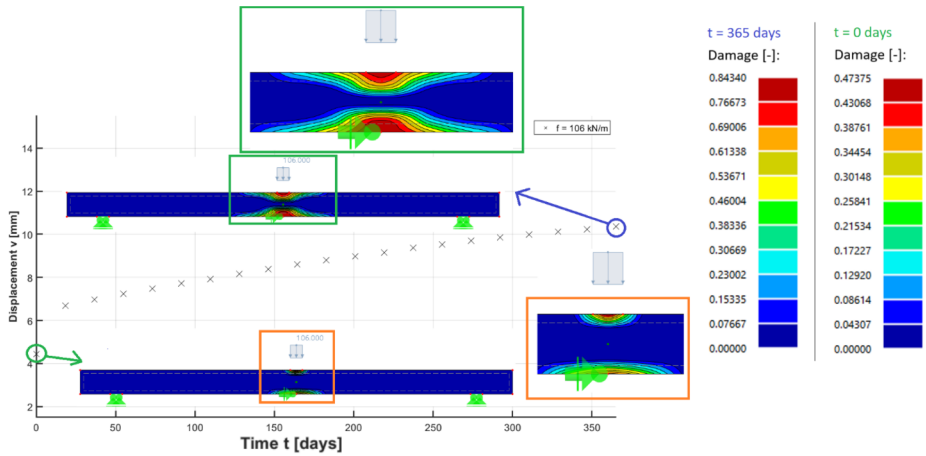


Fig. 13 Damage of the beam in the longitudinal x direction during three-point bending test with line load 106 kN/m at the beginning of loading (0 days, below) and after 365 days of loading (above)(Color figure online)

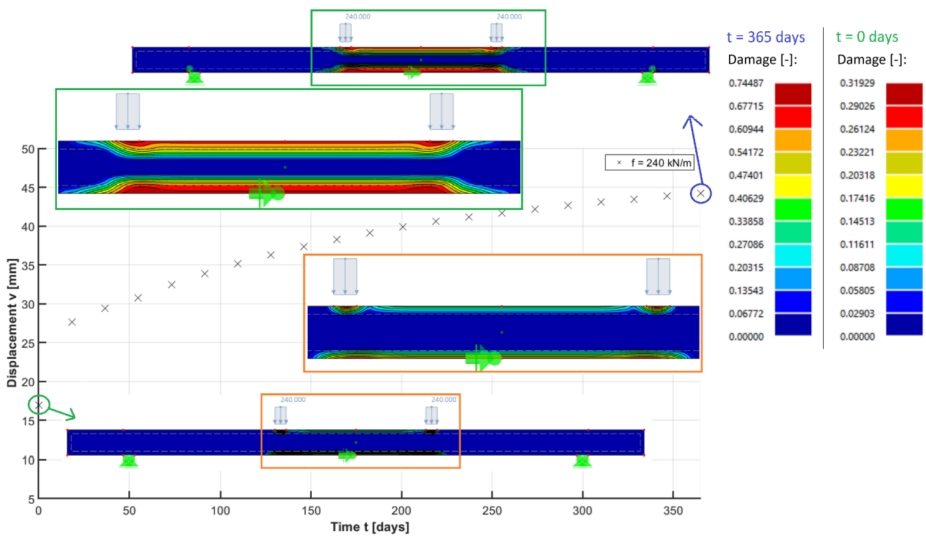


Fig. 14 Damage of the beam in the longitudinal x direction during four-point bending test with two lines load $2 \times 240 \text{ kN/m}$ at the beginning of loading (0 days, below) and after 365 days of loading (above) (Color figure online)

flexion (displacement w in the direction perpendicular to the plane of the plate, i.e., in the z direction) depending on the setting of the material model. The material model would be set in these three variants: a) linear viscoelastic model without the influence of damage (Kelvin chain), b) viscoelastic model combined with a damage model (Kelvin chain + damage model) without consideration of the alpha parameter, c) viscoelastic model combined with a damage model (Kelvin chain + damage model) with a nonzero alpha parameter set to 0.4.

It can be seen from Fig. 6 that the new material model gives the expected results. With the linear viscoelastic model, the deflection is the lowest, in the case of the combined viscoelasticity and damage, a larger deflection even without the influence of the alpha parameter is obtained, and of course, the largest deflection in time occurs while considering the influence of the alpha parameter. If we compare the picture on the left and right sides, it is clear that in the right diagram (plate supported on all four sides), there are smaller deflections and at the beginning (immediately after the application of the load) no damage response occurs (the deflection calculated with the linear material matches the deflection calculated with nonlinear material) and during the loading period, mainly due to the nonzero alpha parameter, the deflections start to differ. On the other hand, on the left figure, slight damage occurs at the beginning (the deflections differ slightly), and this difference increases over time due to the creep. The largest deflections are again for the case of considering the influence of a nonzero alpha parameter.

Figures 7 to 14 show the application of the new material model to the beam deflection (displacement in the y direction) modeled by plane elements as a 2D plane-stress task made on two benchmark tasks: D: three-point beam bending, E: four-point beam bending.

Both benchmark tasks D and E were calculated with three different material model settings: a) the linear viscoelastic model without the influence of the damage (generalized Kelvin chain), b) the viscoelastic model combined with the damage model (Kelvin chain + damage model) without considering the alpha parameter, c) the viscoelastic model in combination with the damage model (Kelvin chain + damage model) with a nonzero alpha parameter set to 0.4.

It can be seen from Fig. 7 that in both cases the deflection of the beam depends on the setting of the material model and the combination of the damage with the creep has a major effect. The greatest influence is again in the case of a nonzero alpha parameter, and the phenomenon called creep damage is demonstrated by comparing the time courses of all the three cases: 1) viscoelastic, 2) viscoelastic + damage, 3) viscoelastic + damage with the alpha parameter.

Figure 8 shows the beam deflection time dependencies for different loading levels f (the material model set to the nonzero value of the parameter $\alpha = 0.4$ to capture the most extreme case of possible behavior – the largest deflections). The aim was to determine for which loading levels the response of the beam is a) without damage in the middle of its length, b) with a slight development of damage in both tension and compression, c) with a largest damage development, d) with a failure of the beam. In both cases, it was shown that the beam may not fail immediately after the application of the load, but only after a certain time. Thus, time plays an important role in the failure of the structure, and to capture the real response of the structure, it is impossible to neglect these viscous phenomena, such as creep in this case. Time curves of the three-point bending test (Fig. 8, left) show that the failure occurs after 109.5 days with the line load of 110 kN/m. Time curves of the four-point bending test show that the failure occurs after 73 days with the two lines load 2×255 kN/m (Fig. 8, right).

Figure 9 shows damage development in the middle of the beam length at its tensile bottom side (i.e., tensile damage in the longitudinal x direction) for loading levels of a) 100 kN/m for the three-point bending (left) and b) 2×250 kN/m for a four-point bending (right). It is observed that in both cases the damage occurs instantaneously after the application of the load and then grows over time. The damage grows more over time for the case of the nonzero alpha.

Figure 10 shows the damage development in the middle of the beam length, at the tensile bottom side (i.e., tensile damage in the longitudinal x direction) for a fixed loading level

(70 kN/m on the left for three-point bending and 2×180 kN/m on the right for four-point bending). In both cases, the damage does not occur instantaneously after the load application, but it occurs after a certain time, and then grows over time. The last case of the material model only is deliberately calculated, when the influence of a nonzero alpha parameter is considered and a smaller loading level is chosen, to show that the damage does not occur immediately after load application but occurs after some time as a result of creep (the so-called creep-damage phenomenon).

The three- and four-point bending test benchmark tasks (Figs. 11, 12, 13, and 14) present the deflection v and the resulting damage parameter in the x direction in the time increments of 0 and 365 days, using the numerical solution of the benchmark problems. The next figures show the deflection v and the damage parameters in the x direction directly connected to the solution time.

Figures 11 and 12 show how the deflection (displacement in the y direction) of the wooden beam that is loaded by the three-point (Fig. 11) and the four-point (Fig. 12) bending increases over time. Shown are the instantaneous deflection after the application of the load (at time $t = 0$ days) and above after one year of loading. All the results are shown for $\alpha = 0.4$. It is observed that the deflection increases significantly with increasing time. This happens for two reasons: a) because of creep itself, but also b) because of a phenomenon called creep damage ($\alpha = 0.4$).

Figures 13 and 14 show the damage distribution inside the wooden beam, which is loaded by the three-point (Fig. 13) and the four-point (Fig. 14) bending. Only the damage component in the longitudinal x -axis direction is shown. At the bottom of the figures, the damage immediately after load application ($t = 0$ days) is shown and at the top, the damage after one year of loading is shown in color at the bottom. All the results are shown for $\alpha = 0.4$. In the upper part of the beam, the compression damage occurs and at the bottom, there is tensile damage. It can be seen in the figure that not only the deflection of the beam (displacement in the y direction) but also the damage increases over time due to creep.

5 Summary and conclusions

In this study, the viscoelastic–damage material model is algorithmized, implemented in the FEM solver, and tested on benchmark tasks. This material model enables the calculation of coupled creep and damage of the orthotropic wood material. The material model is based on a combination of an orthotropic viscoelastic model (generalized Kelvin chain) with the damage model. The combination of these two models is important for a more realistic time-dependent description of the behavior of wood in construction, since wood exhibits not only an instantaneous nonlinear elastic–plastic–damage response but also a time-dependent response due to the viscous nature of the material.

In this work, the phenomenon called creep damage, i.e., damage caused by wood creep, is analyzed. It is shown that: a) damage or plasticity develops over time (grows and spreads further), and that: b) wood may not be damaged or plasticized immediately after loading, but damage or plasticity may occur only after a certain time after loading, and then it develops further.

The results are calculated in three variants: 1) linear viscoelasticity, 2) viscoelasticity combined with the nonlinearity (plasticity or damage) without the influence of the creep-damage alpha parameter (the value of the alpha parameter is set to zero), 3) viscoelasticity combined with the nonlinearity (plasticity or damage) with the influence of the creep-damage alpha parameter (the value of the alpha parameter is set to 0.4). It is shown that the

creep-damage parameter α has a significant influence on the formation and development of plasticity or damage over time and must be considered to capture the real-time-dependent behavior of wood.

The first benchmark tasks A1 and A2 show how the new material model behaves during 1D compressive stress in the elastic–plastic region in the longitudinal and transversal directions when a) plasticization develops over time (grows and spreads further), b) wood does not plasticize immediately after loading, but plasticization can occur only after a certain time after load application, and only then does it develop further.

The second set of tasks (benchmarks B, C) is supplementary, and it aims to show how the new material model behaves in a shell structure under bending load (plate model). For this purpose, a plate is continuously loaded, and it is supported only on two opposite sides, and in the second case, on all four peripheral sides. The results show again that: a) damage or plasticization develops over time (grows and spreads further), and that b) wood does not have to be damaged or plasticized immediately after loading, but the damage or plasticization can occur after a certain time from the load application, later it develops further. Because of the multiaxial stress state in the material (integration) point over the thickness of the shell element, the results are more varied in this task, and it can be observed how, under higher loads, the wood gradually plasticizes (ductilely damages) over time in the places and directions where it is stressed by compression, and in this same task, it can also be observed how it damages in a brittle manner in the points and directions where the wood is stressed by the tension or shear. The results are calculated in the three settings mentioned above.

The last two benchmark problems (D, E) are about the three-point and four-point bending of a beam modeled as a plane problem (2D plane stress) with two normal stress components and one shear stress component. These tasks showed the behavior of the new material model of wood during the bending loading of a wooden beam. The results again showed that: a) damage or plasticization develops over time (grows and spreads further), and that b) wood does not have to be damaged or plasticized immediately after loading, but damage or plasticization can occur only after a certain time from the load, and then it develops further. Because of the multiaxial stress, the results are more varied in this task, and it can be observed how, under higher loads, the wood gradually plasticizes (damaged in a ductile manner) over time in the places and directions where it is stressed by compression, and in this same task, it can also be observed how it damages the wood brittlely in places and directions where the wood is stressed by tension or shear. The results are calculated in the three variants mentioned above.

Finally, the use of the presented modular material model allows us to predict the occurrence and development of the wood damage during a time period, what means that it can be used as a tool for the evaluation of the time-dependent behavior of wooden structures and for prediction of their possible failure. The present study shows the combination of viscoelastic and damage models, but the presented modular approach allows us to include also other phenomena such as damage–plasticity combinations, the influence of moisture and thermal changes (swelling, shrinkage), the influence of cyclic moisture changes (the mechanosorptive creep) or the influence of material fatigue.

Acknowledgements The orthotropic viscoelastic–plastic–damage model was implemented into the FEM solver of the Dlubal RFEM software, which was used also for the benchmark tests.

Author contributions M.T. idea, algorithmization P.S. implementation, benchmarks, manuscript M.B. benchmarks, figures I. N. algorithmization, tutoring All authors reviewed the manuscript.

Funding Open access publishing supported by the National Technical Library in Prague. The manuscript was supported by the Specific University Research Fund of the FFWT Mendel University in Brno, Czech Republic, Project LDF_VP_2020031 Viscoelastic parameters of uniaxially loaded wood. The manuscript was supported by the project of specific university research at Brno University of Technology No. FAST-S-22-7867.

Declarations

Competing interests The authors declare no competing interests.

Open Access This article is licensed under a Creative Commons Attribution 4.0 International License, which permits use, sharing, adaptation, distribution and reproduction in any medium or format, as long as you give appropriate credit to the original author(s) and the source, provide a link to the Creative Commons licence, and indicate if changes were made. The images or other third party material in this article are included in the article's Creative Commons licence, unless indicated otherwise in a credit line to the material. If material is not included in the article's Creative Commons licence and your intended use is not permitted by statutory regulation or exceeds the permitted use, you will need to obtain permission directly from the copyright holder. To view a copy of this licence, visit <http://creativecommons.org/licenses/by/4.0/>.

References

- Bazant, Z.P., Gettu, R.: Rate effects and load relaxation in static fracture of concrete. *ACI Mater. J.* **89**(5), 456–468 (1992)
- Bazant, Z.P., Jirásek, M.: Nonlocal integral formulations of plasticity and damage: survey of progress. *J. Eng. Mech.* **128**(11), 1119–1149 (2002)
- Bazant, Z.P., L'Hermite, R.: Mathematical modeling of creep and shrinkage of concrete (1988)
- Bazant, Z.P., Wu, S.T.: Dirichlet series creep function for aging concrete. *J. Eng. Mech. Div.* **99**(2), 367–387 (1973). <https://doi.org/10.1061/JMCEA3.000174>. ISSN 0044-7951
- Bazant, Z.P., et al.: Pervasive lifetime inadequacy of long-span box girder bridges and lessons for multi-decade creep prediction. In: *Life-Cycle and Sustainability of Civil Infrastructure Systems: Proceedings of the Third International Symposium on Life-Cycle Civil Engineering (IALCCE'12)*, Vienna, Austria, October 3-6, 2012, p. 27. CRC Press, Boca Raton (2012)
- Bazant, Z.P., et al.: Fundamentals of linear viscoelasticity. In: *Creep and Hygrothermal Effects in Concrete Structures*, pp. 9–28 (2018)
- Bengtsson, R., Afshar, R., Gamstedt, E.K.: An applicable orthotropic creep model for wood materials and composites. *Wood Sci. Technol.* **56**(6), 1585–1604 (2022)
- Cannell, M.G.R., Morgan, J.: Young's modulus of sections of living branches and tree trunks. *Tree Physiol.* **3**(4), 355–364 (1987)
- Distéfano, N.: On the identification problem in linear viscoelasticity. *Z. Angew. Math. Mech.* **50**(11), 683–690 (1970). <https://doi.org/10.1002/zamm.19700501106>. ISSN 00442267
- Dlubal Software GmbH: RFEM 6. <https://www.dlubal.com/en/products/rfem-fea-software/what-is-rfem>
- Dufour, F., et al.: Creep-damage coupling. In: *15th US National Congress on Theoretical and Applied Mechanics* (2006)
- Ferry, J.D.: *Viscoelastic Properties of Polymers*. Wiley, New York (1980)
- Fortino, S., Mirianon, F., Toratti, T.: A 3D moisture-stress FEM analysis for time dependent problems in timber structures. *Mech. Time-Depend. Mater.* **13**, 333–356 (2009). <https://doi.org/10.1007/s11043-009-9103-z>
- Hanhijärvi, A., Mackenzie-Helnwein, P.: Computational analysis of quality reduction during drying of lumber due to irrecoverable deformation. I: orthotropic viscoelastic-mechanosorptive-plastic material model for the transverse plane of wood. *J. Eng. Mech.* **129**(9), 975–1105 (2003). [https://doi.org/10.1061/\(ASCE\)0733-9399\(2003\)129:9\(996\)](https://doi.org/10.1061/(ASCE)0733-9399(2003)129:9(996))
- Holzer, S.M., Loferski, J.R., Dillard, D.A.: A review of creep in wood: concepts relevant to develop long-term behavior predictions for wood structures. *Wood Fiber Sci.* **21**(4), 376–392 (1989). ISSN 7356161
- Hunt, D.G.: Linearity and non-linearity in mechano-sorptive creep of softwood in compression and bending. *Wood Sci. Technol.* **23**, 323–333 (1989). <https://doi.org/10.1007/BF00353248>
- Jones, N., Xirouchakis, P.C.: The creep buckling of shells. In: *Creep in Structures: 3rd Symposium*, Leicester, UK, September 8–12, 1980, pp. 308–330. Springer, Berlin (1980)

- Kennedy, J., Eberhart, R.: Particle swarm optimization. In: Proceedings of ICNN'95 – International Conference on Neural Networks [Online], pp. 1942–1948. IEEE, Los Alamitos (1995). ISBN 0-7803-2768-3. <https://doi.org/10.1109/ICNN.1995.488968>
- Kennedy, J., Eberhart, R.: Particle swarm optimization. In: Proceedings of ICNN'95 – International Conference on Neural Networks [Online], pp. 1942–1948. IEEE, Los Alamitos (1995). ISBN 0-7803-2768-3. <https://doi.org/10.1109/ICNN.1995.488968>
- Liu, T.: Creep of wood under a large span of loads in constant and varying environments. *Holz Roh- Werkst.* **52**, 63–70 (1994). <https://doi.org/10.1007/BF02615022>
- Maimí, P., et al.: A thermodynamically consistent damage model for advanced composites (2006)
- Maimí, P., et al.: A continuum damage model for composite laminates: part I—constitutive model. *Mech. Mater.* **39**(10), 897–908 (2007)
- Massaro, F.M., Malo, K.A.: Long-term behaviour of Norway spruce glulam loaded perpendicular to grain. *Eur. J. Wood Wood Prod.* **77**, 821–832 (2019). <https://doi.org/10.1007/s00107-019-01437-4>
- Massaro, F.M., Malo, K.A.: Modelling the viscoelastic mechanosorptive behaviour of Norway spruce under long-term compression perpendicular to the grain. *Holzforchung* **73**(8), 715–725 (2019). <https://doi.org/10.1515/hf-2018-0218>
- Matzenmiller, A., Lubliner, J., Taylor, R.L.: A constitutive model for anisotropic damage in fiber-composites. *Mech. Mater.* **20**(2), 125–152 (1995)
- Mazzotti, C., Savoia, M.: Nonlinear creep damage model for concrete under uniaxial compression. *J. Eng. Mech.* **129**(9), 1065–1075 (2003)
- Moll, I., Navrátil, J., Žák, J.: Výpočet exponentů při aproximaci funkce součtem exponenciál. In: Knižnice algoritmov XI Proceedings of Sympóziium Algoritmy '91, 15.-19.4.1991, pp. 11–16. Štrbské pleso, Slovensko. JSMF SAV: Bratislava. (1991) https://doi.org/10.1007/978-94-024-1138-6_2
- Omar, M., et al.: Creep loading influence on the residual capacity of concrete structure: experimental investigation. In: Fifth International Conference on Fracture Mechanics of Concrete and Concrete Structures (2004)
- Omar, M., et al.: Creep-damage coupled effects: experimental investigation on bending beams with various sizes. *J. Mater. Civ. Eng.* **21**(2), 65–72 (2009)
- Ozyhar, T., Hering, S., Niemz, P.: Viscoelastic characterization of wood: time dependence of the orthotropic compliance in tension and compression. *J. Rheol.* **57**(2), 699–717 (2013). <https://doi.org/10.1122/1.4790170>. ISSN 0148- 6055
- Pister, K.S.: Mathematical modeling for structural analysis and design. *Nucl. Eng. Des.* **18**(3), 353–375 (1972). [https://doi.org/10.1016/0029-5493\(72\)90108-2](https://doi.org/10.1016/0029-5493(72)90108-2). ISSN 00295493
- Saliba, J., et al.: Relevance of a mesoscopic modeling for the coupling between creep and damage in concrete. *Mech. Time-Depend. Mater.* **17**, 481–499 (2013)
- Sandhaas, C., Sarnaghi, A.K., van de Kuilen, J.-W.: Numerical modelling of timber and timber joints: computational aspects. *Wood Sci. Technol.* **54**, 31–61 (2020)
- Schniewind, A.P.: Recent progress in the study of the rheology of wood. *Wood Sci. Technol.* **2**, 188–206 (1968). <https://doi.org/10.1007/BF00350908>
- Shi, Y., Eberhart, R.C.: Parameter selection in particle swarm optimization. In: Porto, V.W., Saravanan, N., Waagen, D., Eiben, A.E. (eds.) *Evolutionary Programming VII* [Online]. Lecture Notes in Computer Science, pp. 591–600. Springer, Berlin (1998). ISBN 978-3-540-64891-8. <https://doi.org/10.1007/BFb0040810>
- Shi, Y., Eberhart, R.C.: Parameter selection in particle swarm optimization. In: Porto, V.W., Saravanan, N., Waagen, D., Eiben, A.E. (eds.) *Evolutionary Programming VII* [Online]. Lecture Notes in Computer Science, pp. 591–600. Springer, Berlin (1998). ISBN 978-3-540-64891-8. <https://doi.org/10.1007/BFb0040810>
- Toratti, T.: Creep of Timber Beams in a Variable Environment. Doctoral dissertation, Helsinki University of Technology, Espoo (1992)
- Yu, Q., Bazant, Z.P., Wendner, R.: Improved algorithm for efficient and realistic creep analysis of large creep-sensitive concrete structures. *ACI Struct. J.* **109**(5), 665 (2012)